

1 **Bioactive zinc-doped sol-gel coating modulates protein adsorption patterns and *in vitro***
2 **cell responses**

3 A. Cerqueira^{1#}, F. Romero-Gavilán^{1*#}, I. García-Arnáez², C. Martínez-Ramos³, S. Ozturan⁴, I.
4 Iloro⁵, M. Azkargorta⁵, F. Elortza⁵, R. Izquierdo¹, M. Gurruchaga², I. Goñi², J. Suay¹

5 ¹Department of Industrial Systems Engineering and Design, Universitat Jaume I, Av. Vicent
6 Sos Baynat s/n, 12071 Castellón de la Plana, Spain

7 ²Departament of Science and Technology of Polymers, Universidad del País Vasco, P. M. de
8 Lardizábal, 3, 20018 San Sebastián, Spain

9 ³Center for Biomaterials and Tissue Engineering, Universitat Politècnica de Valencia, Camino
10 de Vera, s/n 46022 Valencia, Spain

11 ⁴Department of Periodontology, Faculty of Dentistry, Istanbul Medeniyet University, Istanbul,
12 Turkey

13 ⁵Proteomics Platform, CIC bioGUNE, Basque Research and Technology Alliance (BRTA),
14 CIBERehd, ProteoRed-ISCI, Bizkaia Science and Technology Park, 48160 Derio, Spain

15

16 #Co-authorship

17 *Corresponding author: Francisco Romero-Gavilán

18

19 Departamento de Ingeniería de Sistemas Industriales y Diseño

20 Campus del Riu Sec

21 Avda. Vicent Sos Baynat s/n

22 12071 – Castelló de la Plana (España)

23 E-mail: gavilan@uji.es

24

25

26

27 **Abstract**

28 Zinc is an essential element with an important role in stimulating the osteogenesis and
29 mineralization and suppressing osteoclast differentiation. In this study, new bioactive ZnCl₂-
30 doped sol-gel materials were designed to be applied as coatings onto titanium. The biomaterials
31 were physicochemically characterized and the cellular responses evaluated *in vitro* using
32 MC3T3-E1 osteoblasts and RAW264.7 macrophages. The effect of Zn on the adsorption of
33 human serum proteins onto the material surface was evaluated through nLC-MS/MS. The
34 incorporation of Zn did not affect the crosslinking of the sol-gel network. A controlled Zn²⁺
35 release was obtained, reaching values below 10 ppm after 21 days. The materials were not
36 cytotoxic and led to increased gene expression of ALP, TGF-β, and RUNX2 in the osteoblasts.
37 In macrophages, an increase of IL-1β, TGF-β, and IL-4 gene expression was accompanied by
38 a reduced TNF-α liberation. Proteomic results showed changes in the adsorption patterns of
39 proteins associated with immunological, coagulative, and regenerative functions, in a Zn dose-
40 dependent manner. The variations in protein adsorption might lead to the downregulation of the
41 NF-κB pathway, thus explaining the observed biological effects of Zn incorporation into
42 biomaterials. Overall, these coatings demonstrated their potential to promote bone tissue
43 regeneration.

44

45 **Keywords**

46 Proteomics, Bioinorganic Chemistry, Biomaterials, Bone Regeneration, Hybrids

47

48 **1. Introduction**

49 As an essential trace element, zinc (Zn) plays an important physiological role in the human
50 body, performing various functions in growth, immunity, tissue maintenance, and wound
51 healing [1]. Most of the Zn is stored in bone tissue, mainly as a component of the calcified
52 matrix [2]. It plays a pivotal role in bone metabolism and remodeling [3], supporting
53 osteoblastogenesis, and suppressing osteoclastogenesis [4]. Zinc can enhance osteogenesis and
54 mineralization by activating the aminoacyl-RNA synthesis in osteoblastic cells [5], and
55 stimulating the alkaline phosphatase (ALP) activity and collagen synthesis in a dose-dependent
56 manner [6]. However, this divalent cation can also downregulate osteoclast differentiation due
57 to its effect on the RANKL/RANK/OPG signaling pathway [7]. Zinc deficiency causes various
58 diseases and skeletal abnormalities during fetal and postnatal development, such as bone growth
59 retardation, abnormal mineralization, and osteoporosis [8]. Zinc is also known for its
60 antioxidant and anti-inflammatory properties; it is used as a therapeutic agent in chronic
61 diseases [9]. Moreover, Zn inhibits the induction of TNF- α and IL-1 β in monocytes and
62 prevents the TNF- α -induced NF- κ B activation [10].

63 The intrinsic physiological relevance of this element has attracted the interest of researchers in
64 the biomaterial field; its incorporation into bone-engineered materials could enhance the desired
65 regenerative properties. Zinc-doped degradable materials such as hydroxyapatites, bioglasses,
66 and metallic alloys have recently emerged demonstrating pro-regenerative capabilities [11,12].
67 However, delayed osseointegration induced by excessive release of Zn²⁺ ions has been observed
68 in pure Zn-ion implants [5]. Thus, the control of the degradation product release is necessary to
69 ensure the biosafety of these materials and optimize their therapeutic effects [13].

70 Immediately after implantation, a material interacts with surrounding tissues and fluids. A
71 complex sequence of events is initiated in order to promote tissue repair and determine
72 integration/rejection of the introduced foreign body [14,15]. The interaction between the
73 biomaterial and body fluids, such as the blood, results in the adsorption of proteins onto the
74 surface of the implant. These proteins compete against each other by a displacement mechanism
75 known as the Vroman effect [16]. The regenerative processes, such as inflammation,
76 coagulation, fibrinolysis, and angiogenesis, will depend on the type of proteins attached to the
77 material [17,18]. Inflammation is one of the first reactions to implantation, playing a pivotal
78 role in tissue regeneration, and can condition the subsequent responses to the implant [17,19].
79 Depending on the intensity of the inflammatory response, it can be initiated the regeneration

80 process by recruitment of the mesenchymal cells and boosting of the osteogenesis, or it can be
81 triggered a foreign body reaction, causing the implant rejection [20,21].

82 This study aimed to synthesize and characterize a new organic-inorganic sol-gel release vehicle
83 doped with Zn ions to be applied as coatings onto titanium. The materials were
84 physiochemically characterized and the effects of Zn^{2+} on protein adsorption were studied using
85 proteomic analysis. Also, *in vitro* assays of cell behavior were conducted using MC3T3-E1
86 osteoblast and RAW 264.7 macrophage cell lines. The correlation between the cellular
87 responses and the Zn dose-dependent protein adsorption patterns will allow to better understand
88 the role of this element in bone tissue regeneration.

89 **2. Materials and methods**

90 *2.1. Substrate*

91 Grade- 4 Ti discs, 1-mm thick, 12 mm in diameter (Ilerimplant-GMI SL., Lleida, Spain), were
92 employed as a substrate for the coatings. Disc surfaces were first modified using the
93 sandblasting and acid-etching treatment (SAE) described in the previous study [22] and
94 sterilized with UV radiation.

95 *2.2. Sol-gel synthesis and coating preparation*

96 The Zn-containing hybrid materials were developed using the sol-gel synthesis. Organically
97 modified alkoxysilanes, methyltrimethoxysilane (MTMOS; M) and tetraethyl orthosilicate
98 (TEOS; T), were employed as precursors. The proportion of these reagents was 70 % of M to
99 30 % of T (molar ratio), as described in previous studies [23]. The solvent used in the synthesis
100 was 2-Propanol (volume ratio of alcohol to siloxane, 1:1). The precursor hydrolysis was
101 conducted by adding the corresponding stoichiometric amount of H_2O at a rate of 1 drop s^{-1} .
102 The water was acidified with HNO_3 (0.1 M) to catalyze the sol-gel reactions. An appropriate
103 amount of $ZnCl_2$ was dissolved in this solution for its incorporation into the sol-gel mixture.
104 The preparations were kept for 1 h under stirring and then 1 h at rest at room temperature. Four
105 different compositions were synthesized: the sol-gel network without Zn (MT; control) and
106 enriched with 0.5, 1, and 1.5 wt % $ZnCl_2$ (designated as MT0.5Zn, MT1Zn, and MT1.5Zn,
107 respectively). The mass percentages were relative to the total amount of alkoxysilane. Also,
108 SAE uncoated titanium samples (Ti) were used as controls. All the reagents employed for the
109 synthesis were purchased from Sigma-Aldrich (Merck KGaA, Darmstadt, Germany). The
110 samples were prepared immediately after finishing the sol-gel synthesis. The coatings were

111 applied onto the SAE-Ti discs with a dip-coater (KSV DC; KSV NIMA, Espoo, Finland). The
112 discs were immersed in the sol-gel solutions at a speed of 60 cm min^{-1} , left immersed for one
113 minute, and removed at a 100 cm min^{-1} . To evaluate the hydrolytic degradation and Zn^{2+}
114 release, glass slides were used as a substrate for the coatings. The glass surfaces were first
115 cleaned with HNO_3 solution (25 % v/v) in an ultrasonic bath (Sonoplus HD 3200) for 20 min
116 at 30 W. A second wash with distilled water was performed under the same conditions. Then,
117 the samples were coated by casting, adding the same amount of sol-gel in all cases. To carry
118 out the chemical analyses, free films of the materials were obtained by pouring the sol-gel
119 solutions into non-stick Teflon molds. Finally, all the samples were cured for 2 h at $80 \text{ }^\circ\text{C}$.

120 *2.3. Physicochemical characterization*

121 The morphology of the obtained coatings was analyzed using SEM with a Leica-Zeiss LEO
122 equipment, under vacuum (Leica, Wetzlar, Germany). Platinum sputtering was used to increase
123 the coating conductivity for the SEM examination. Fourier-transform infrared spectroscopy
124 (FTIR; Thermo Nicolet 6700 spectrometer, Thermo Fisher Scientific, Waltham, MA, USA)
125 with an attenuated total reflection system (ATR) was employed for chemical characterization
126 of the synthesized materials. The spectra were recorded in the 400 to 4000 cm^{-1} wavelength
127 range. The level of structural crosslinking was studied using silicon solid-state nuclear magnetic
128 resonance spectroscopy ($^{29}\text{Si-NMR}$). To achieve this, a Bruker 400 Avance III WB Plus
129 spectrometer (Bruker, Billerica, MA, USA) with a cross-polarization magic-angle spinning
130 (CP-MAS) probe for solid samples was employed. The pulse sequence for the analysis was the
131 Bruker standard: 79.5 MHz frequency, 55 kHz spectral width, 2 ms contact time and 5 s delay
132 time. The spinning speed was 7.0 kHz. The surface roughness of the developed coatings was
133 measured using an optical profilometer (interferometric and confocal) PLm2300 (Sensofar,
134 Barcelona, Spain). Three discs were tested for each condition. Three measurements were
135 performed for each disc to obtain an average Ra (arithmetic average roughness parameter).

136 The wettability was characterized using contact angle measurements, employing an automatic
137 contact angle meter OCA 20 (Dataphysics Instruments, Filderstadt, Germany). Drops of $10 \text{ }\mu\text{L}$
138 of ultrapure water were deposited on the material surfaces at a $27.5 \text{ }\mu\text{L s}^{-1}$ dosing rate. Contact
139 angles were determined using SCA 20 software (DataPhysics Instruments). Six discs of each
140 material were studied, after depositing two drops on each disc.

141 Hydrolytic degradation of the coatings was examined by measuring the sol-gel mass loss after
142 incubation in 50 mL of distilled water at $37 \text{ }^\circ\text{C}$ for 7, 14, 28, 49, and 63 days. The degradation

143 of the coatings was registered as the percentage of the original mass lost. Three different
144 samples were used for each condition. The Zn^{2+} release kinetics were measured using an
145 inductively coupled plasma mass spectrometer (Agilent 7700 Series ICPMS; Agilent
146 Technologies, Santa Clara, CA, USA). Samples were incubated in ddH₂O at 37 °C for 21 days.
147 Aliquots of 0.5 mL were removed after 2, 4, 8, 168, 336, and 504 h of immersion. Each data
148 point is the average of three individual measurements.

149 *2.4. In vitro assays*

150 *2.4.1. Cell culture*

151 Mouse calvaria osteosarcoma (MC3T3-E1) cell line was cultured on the discs at a concentration
152 of 1.75×10^4 cells cm⁻² for 7 and 14 days. For the first 24 h, the culture medium was composed
153 of low-glucose DMEM (Gibco, Thermo Fisher Scientific) supplemented with 1 %
154 penicillin/streptomycin (Biowest Inc., Riverside, MO, USA) and 10 % FBS (Gibco). The
155 samples were kept in a cell incubator (90 % humidity, 37 °C, 5 % CO₂). Then, the cell culture
156 medium was replaced with osteogenic medium (DMEM, 1 % of penicillin/streptomycin, 10 %
157 FBS, 1 % ascorbic acid (50 µg mL⁻¹), and 100 mM β-glycerol phosphate), which was changed
158 every two days.

159 Mouse murine macrophage (RAW264.7) cell line was cultured on the materials at a
160 concentration of 30×10^4 cells cm⁻² for 2 and 4 days in high-glucose DMEM supplemented with
161 1 % penicillin/streptomycin and 10 % FBS in a cell incubator (90 % humidity, 37 °C, 5 % CO₂).

162 *2.4.2. Cytotoxicity, proliferation, and ALP activity*

163 To evaluate the cytotoxicity of biomaterials, the ISO 10993-5:2009 (Annex C) norm [24] was
164 followed. Samples were prepared according to the ISO 10993-12:2012 norm [25]. MC3T3-E1
165 cells were seeded and incubated in 96-well NUNC plates (Thermo Fisher Scientific) for 24 h.
166 For serum extraction, the materials were incubated in cell culture medium for the same period.
167 Then, the cells were exposed to the material extract for another 24 h. Based on the formazan
168 formation, the CellTiter 96® Proliferation Assay (MTS; Promega, Madison, WI) was used
169 according to manufacturer's guidelines. The negative control was composed of wells with only
170 cells and the cells incubated with latex (cytotoxic compound) constituted the positive control.
171 A material would be considered cytotoxic if the cell viability fell below 70 %.

172 To measure the effects of the tested biomaterials on proliferation, MC3T3-E1 cells were
173 cultured on the discs for 1, 3, and 7 days and the alamarBlue™ cell viability reagent (Invitrogen,
174 Thermo Fisher Scientific) was used following the manufacturer's protocol.

175 The ALP activity was measured, following the protocol of Araújo-Gomes *et al.* [20], to evaluate
176 the effect of the Zn-enriched materials on cell mineralization. Briefly, the MC3T3-E1 cells were
177 seeded onto different disc surfaces in 48-well NUNC plates (Thermo Fisher Scientific). After
178 culturing for 7 and 14 days, lysis buffer (0.2 % Triton X-100, 10 mM Tris-HCl, pH 7.2) was
179 added. Then, 100 µL of *p*-NPP (1mg mL⁻¹) in substrate buffer (50 mM glycine, 1 mM MgCl₂,
180 pH 10.5) was added to the samples. After 2 h of incubation, the absorbance at 405 nm was
181 measured using a microplate reader. The ALP activity was obtained using the standard curve
182 of *p*-nitrophenol in 0.02 mM sodium hydroxide. It was normalized to protein content obtained
183 employing a Pierce BCA assay kit (Thermo Fisher Scientific).

184 2.4.3. Cytokine quantification by ELISA

185 The level of tumor necrosis factor (TNF-α) was measured in the culture medium of RAW264.7
186 cells incubated on the discs for 2 and 4 days. Its concentration was determined using an ELISA
187 (Invitrogen, Thermo Fisher Scientific) kit following the manufacturer's instructions.

188 2.4.4. Relative gene expression: RNA extraction, cDNA synthesis, and qRT-PCR

189 For total RNA extraction, MC3T3-E1 cells were grown on the tested materials for 7 and 14
190 days, and RAW264.7 for 2 and 4 days. The assays were carried out in 48-well NUNC plates
191 (Thermo Fisher Scientific). At each time point, RNA was extracted using TRIzol as described
192 in Cerqueira *et al.* [26]. RNA concentration, integrity, and quality were measured employing
193 NanoVue® Plus spectrophotometer (GE Healthcare Life Sciences, Little Chalfont, UK).

194 For cDNA synthesis, approximately 1 µg of total RNA was converted into cDNA using
195 PrimeScript RT Reagent Kit (Perfect Real-Time; TAKARA Bio Inc., Shiga, Japan). The
196 reaction was carried out under the following conditions: 37 °C for 15 min, 85 °C for 5 secs, and
197 a final hold at 4 °C. The resulting cDNA was diluted in DNase-free water to a concentration
198 suitable for gene expression evaluation. Quantitative real-time PCR (qRT-PCR) was carried out
199 in 96-well plates (Applied Biosystems®, Thermo Fisher Scientific) for the genes of interest and
200 the housekeeping gene (*GAPDH*). Primers were designed using PRIMER3plus software tool
201 from sequences obtained from NCBI Nucleotide and purchased from Thermo Fisher Scientific.
202 Targets are shown in **Table 1**. Individual qRT-PCR reactions contained 1 µL of cDNA, 0.2 µL

203 of specific primers (forward and reverse, at 10 μ M concentration) and 5 μ L of SYBR Premix
 204 Ex Taq (Tli RNase H Plus; TAKARA), in a final volume of 10 μ L. Reactions were carried out
 205 in a StepOnePlus™ Real-Time PCR System (Applied Biosystems®, Thermo Fisher Scientific).
 206 Fold changes were calculated using the $2^{-\Delta\Delta C_t}$ method and data normalized to the wells without
 207 any material.

208 **Table 1.** Targets studied in MC3T3-E1 and RAW264.7.

Gene	Accession	Sequence	Product length
<i>GADPH</i>	XM_017321385	F: TGCCCCCATGTTTGTGATG R: TGGTGGTGCAGGATGCATT	83
<i>ALP</i>	XM_006538499	F: CGGGACTGGTACTCGGATAA R: ATTCCACGTCGGTTCTGTTC	157
<i>TGFβ</i>	NM_011577	F: TTGCTTCAGCTCCACAGAGA R: TGGTTGTAGAGGGCAAGGAC	183
<i>iNOS</i>	NM_001313922	F: CACCTTGGAGTTCACCCAGT R: ACCACTCGTACTTGGGATGC	170
<i>RUNX2</i>	NM_001271631	F: CCCAGCCACCTTTACCTACA R: TATGGAGTGCTGCTGGTCTG	150
<i>RANKL</i>	AF019048	F: AGCCGAGACTACGGCAAGTA R: GCGCTCGAAAGTACAGGAAC	208
<i>RANK</i>	AF019046	F: GCTGGCTACCACTGGAAGTTC R: GTGCAGTTGGTCCAAGGTTT	182
<i>TNF-α</i>	NM_001278601	F: AGCCCCCAGTCTGTATCCTT R: CTCCCTTTCAGAACTCAGG	212
<i>IL-1β</i>	NM_008361	F: GCCCATCCTCTGTGACTCAT R: AGGCCACAGGTATTTTGTCG	230
<i>IL-4</i>	NM_021283	F: TCAACCCCCAGCTAGTTGTC R: TGTTCTTCGTTGCTGTGAGG	177

209

210 2.4.5. Protein layer elution and proteomic analysis

211 The protein layers on the distinct sol-gel formulations were examined after their incubation in
 212 a humidified atmosphere (37 °C, 5 % CO₂) for 3 h with 1 mL of human blood serum from male

213 AB plasma (Sigma-Aldrich). The serum was removed, and non-adsorbed proteins were
214 eliminated by five consecutive washes with ddH₂O and another with 100 mM NaCl, 50 mM
215 Tris-HCl, pH 7.0. The adsorbed proteins were eluted by washing the surfaces with 0.5 M
216 triethylammonium bicarbonate buffer (TEAB), with 4 % sodium dodecyl sulfate (SDS) and 100
217 mM-dithiothreitol (DTT). The experiment was performed in quadruplicate for each material,
218 and each of these replicas was the result of pooling four different processed samples. The total
219 protein content of the serum was measured before the assay, obtaining a value of 51 mg mL⁻¹.

220 The eluted proteins were characterized using electrospray tandem mass spectrometry,
221 employing a nanoACQUITY UPLC (Waters, Milford, MA, USA) coupled to an Orbitrap XL
222 (Thermo Electron, Bremen, Germany). The protocol described by Romero-Gavilán *et al.* [15]
223 was followed. Each condition was analyzed in quadruplicate. Proteomic results were examined
224 using PEAKS (Bioinformatics Solutions Inc., Waterloo, Canada). Functional classification of
225 the identified proteins was performed using DAVID Go annotation (<https://david.ncifcrf.gov/>)
226 and PANTHER programs (<http://www.pantherdb.org/>).

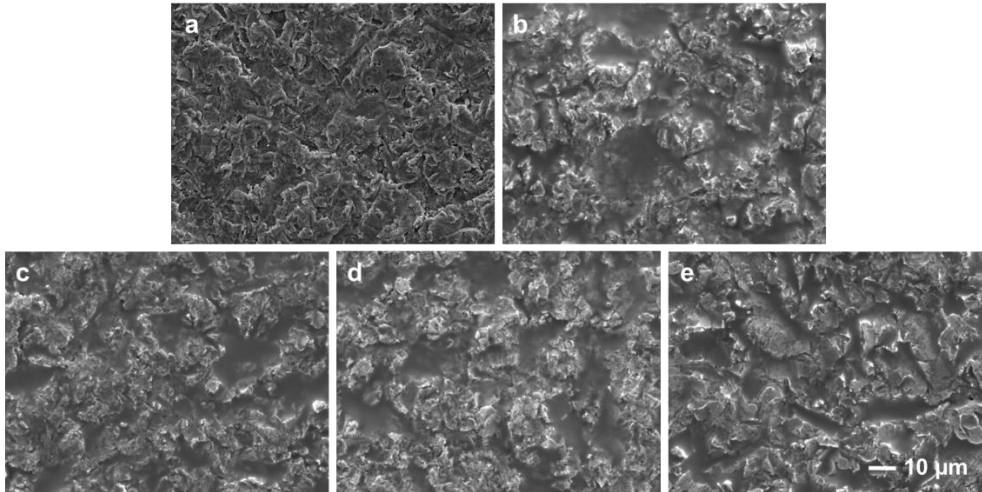
227 2.5. Statistical analysis

228 Physicochemical characterization and *in vitro* assay data, after evaluation of the normal
229 distribution and equal variances, were submitted to one-way analysis of variance (ANOVA)
230 with Tukey *post-hoc* test. Statistical analysis was performed using SigmaPlot v. 12.5 software
231 for Windows (Systat Software Inc., Chicago, IL, USA). The differences between the MT
232 materials and MT enriched with Zn were considered statistically significant at $p \leq 0.05$ (*), $p \leq$
233 0.01 (**), and $p \leq 0.001$ (***). Data were expressed as mean \pm standard error (SE). For
234 proteomic analysis, Student's *t*-test was performed, and protein adsorption differences were
235 considered statistically significant at $p \leq 0.05$ and a ratio higher than 1.3 in either direction.

236 3. Results

237 3.1. Physicochemical characterization

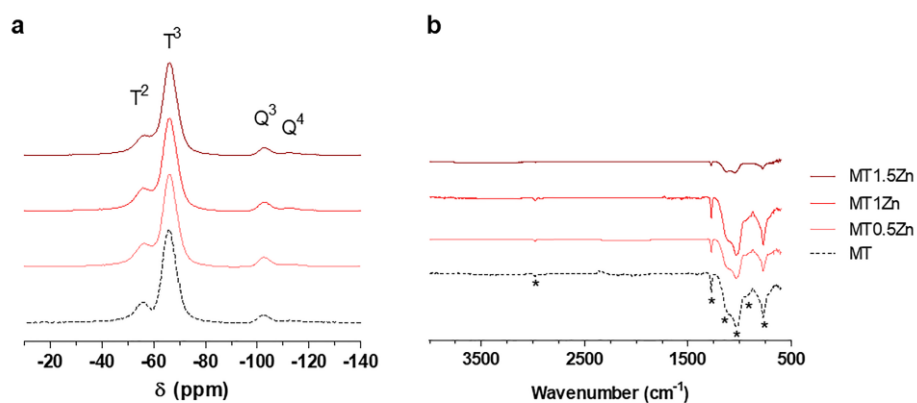
238 The organic-inorganic sol-gel materials with increasing amounts of ZnCl₂ were successfully
239 synthesized and applied as coatings onto the Ti discs. As can be seen in SEM micrographs (**Fig.**
240 **1**), no cracks or holes resulting from the curing process were detected. Moreover, no salt
241 precipitates were observed, so the ZnCl₂ was correctly incorporated into the sol-gel network.



242

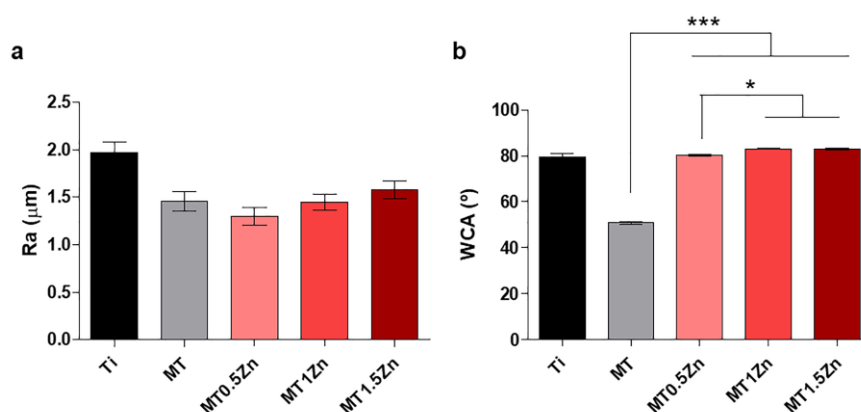
243 **Fig. 1.** SEM microphotograph of SAE-Ti (a), MT (b), MT0.5Zn (c), MT1Zn (d) and MT1.5Zn
 244 (e). Scale bar, 10 μm .

245 The obtained sol-gel materials were chemically characterized using ^{29}Si -NMR and FT-IR (**Fig.**
 246 **2**). The ^{29}Si -NMR spectra showed no effects on the silica network condensation with the ZnCl_2
 247 addition (**Fig. 2a**). The signals detected in the range between -50 and -70 ppm can be assigned
 248 to the MTMOS trifunctional precursor (T units - $\text{CH}_3\cdot\text{SiO}_3$). The signals between - 97.5 and -
 249 115 ppm represent the TEOS tetrafunctional alkoxy silane (Q units - SiO_4) [27]. Thus, the
 250 signals at -56 and -66 ppm indicate the presence of T^2 and T^3 species, while chemical shifts at
 251 -102 and -110 ppm can be associated with the formation of Q^3 and Q^4 structures, respectively
 252 [28]. In general, the networks reached a high degree of MTMOS crosslinking as T^3 signal was
 253 more intense than T^2 , and no T^0 or T^1 shifts were observed. Similarly, no Q^0 , Q^1 or Q^2 TEOS
 254 species were identified although, in this case, the level of condensation was probably lower as
 255 Q^3 peak was larger than Q^4 . The FT-IR results are displayed in **Fig. 2b**. Bands at 780, 1020 and
 256 1125 cm^{-1} associated with the polysiloxane chain vibration reveal the formation of Si-O-Si
 257 bonds during the sol-gel synthesis [29]. The band at 950 cm^{-1} indicates the presence of non-
 258 condensed Si-OH species [30]. The methyl group integrity in the sol-gel structure is confirmed
 259 by its characteristics bands at 1265 and 2980 cm^{-1} , which are attributed to the Si-C and C-H
 260 bonds, respectively [29].



261
 262 **Fig. 2.** ^{29}Si MAS-NMR (a) and FTIR (b) spectra of sol-gel networks MT, 0.5MTZn, MT1Zn,
 263 and MT1.5Zn.

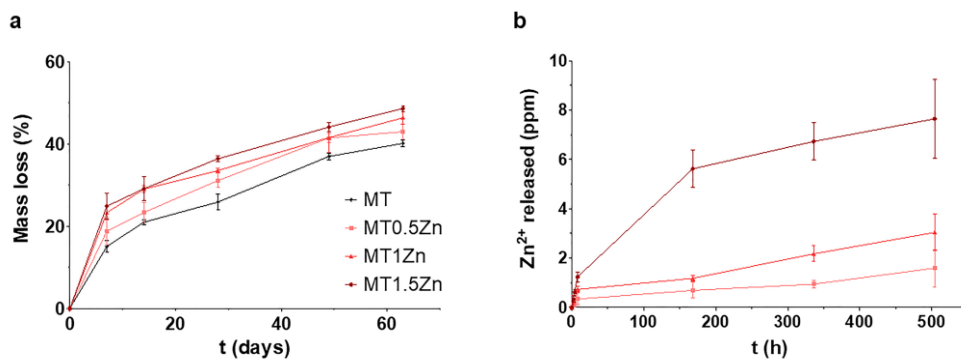
264 The surface roughness was evaluated using the Ra parameter. **Fig. 3a** shows that the
 265 incorporation of ZnCl_2 into the coatings did not change their Ra values (in comparison with the
 266 material without Zn) significantly. **Fig. 3b** displays the contact angle measurements. The
 267 addition of ZnCl_2 to the MT network, resulting in the reduction in surface hydrophilicity, caused
 268 a significant increase in the contact angle values.



269
 270 **Fig. 3.** The arithmetic average of roughness (Ra; a) and contact angle (WCA; b). Results are
 271 shown as mean \pm SE. The asterisks ($p \leq 0.05$ (*) and $p \leq 0.001$ (***)) indicate the statistical
 272 significance of differences between the materials with and without Zn (MT).

273 The hydrolytic degradation kinetics of the tested sol-gel materials are shown in **Fig. 4a**. In
 274 general, all the formulations showed the highest mass-loss rates during the first week of
 275 incubation in water. Nevertheless, their degradation increased throughout the test period (63
 276 days); reaching mass loss values of approximately 40 % of the initial mass. The hydrolytic
 277 degradation of sol-gel coatings intensified with an increase in ZnCl_2 content. A continuous

278 release of Zn^{2+} was observed until the end of the assay, at 21 days (**Fig. 4b**). The largest amounts
 279 of Zn^{2+} were released from the material with the highest proportion of $ZnCl_2$ in the MT network.

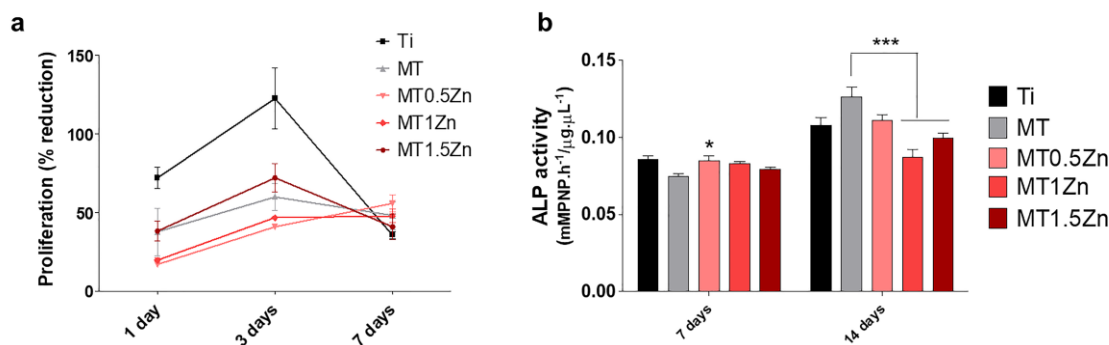


280
 281 **Fig. 4.** Hydrolytic degradation (a) and cumulative Zn^{2+} release (b) for the MT sol-gels doped
 282 with $ZnCl_2$. Bars indicate standard errors.

283 3.2. *In vitro* assays

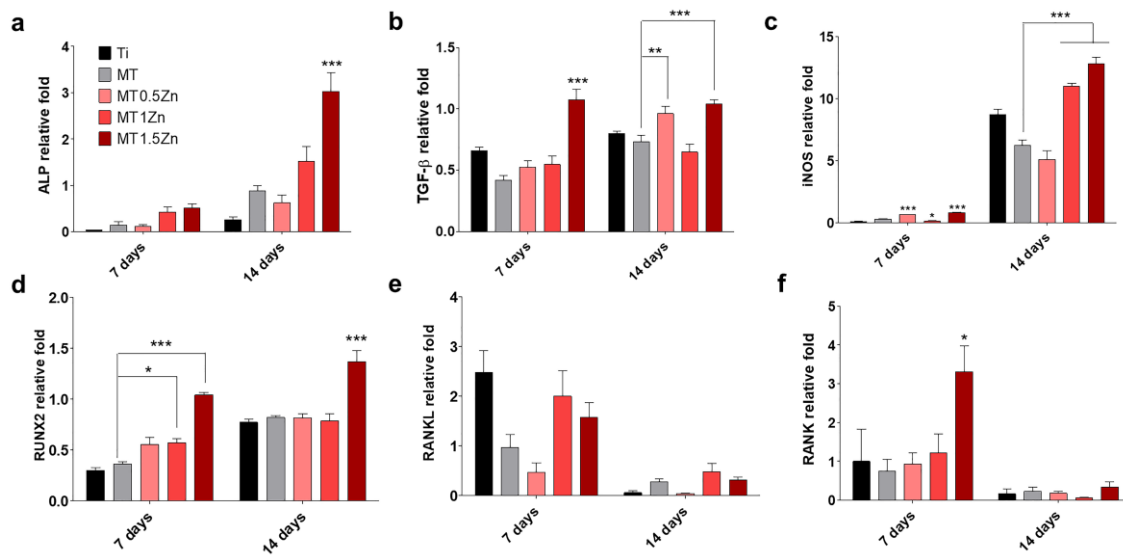
284 3.2.1. Osteogenic responses: effects on osteoblastic cells

285 None of the materials tested were cytotoxic (**Supplementary Fig. 1**). In tests of cell
 286 proliferation, a peak in cell growth was observed after 3 days in all cases, but no significant
 287 differences were found for any of the studied coatings (**Fig. 5a**). The mineralization levels,
 288 evaluated by examining the ALP activity, showed a significant increase for MT0.5Zn after 7
 289 days, in comparison with the MT. After 14 days, there was a general increase in the ALP
 290 activity; however, it was significantly lower for the MT1Zn and MT1.5Zn materials in
 291 comparison with the MT (**Fig. 5b**).



292
 293 **Fig. 5.** MC3T3-E1 (a) cell proliferation after 1, 3, and 7 days and (b) ALP activity after 7 and
 294 14 days. Results are shown as mean \pm SE. The asterisks ($p \leq 0.05$ (*) and $p \leq 0.001$ (***))
 295 indicate statistically significant differences between the materials with Zn and the coating
 296 without Zn (MT).

297 To evaluate how Zn-enriched sol-gel coatings affect osteogenesis, gene expression was
 298 measured in MC3T3-E1 cells (**Fig. 6**). An increase in TGFβ expression was observed on
 299 MT1.5Zn coating after 7 days (**Fig. 6b**). After 14 days, there was an increase in ALP expression
 300 on MT1.5Zn and TGFβ expression levels on MT0.5Zn and MT1.5Zn coatings (**Fig. 6a and**
 301 **6b**). In what concerns iNOS (**Fig. 6c**), an increase of these markers was detected at 7 days in
 302 MT0.5Zn and MT1.5Zn, while MT1Zn showed a significant decrease. After 14 days, this
 303 marker was increased in MT1Zn and MT1.5Zn. In the markers related to osteoclastogenesis,
 304 RUNX2 showed an increase in MT1Zn and MT1.5Zn at 7 days (**Fig. 6d**), while MT1.5Zn lead
 305 to an increase of RANK in the same time point (**Fig. 6f**). At 14 days, RUNX2 was significantly
 306 more expressed in MT1.5Zn. RANKL expression showed no differences between materials
 307 (**Fig. 6e**).

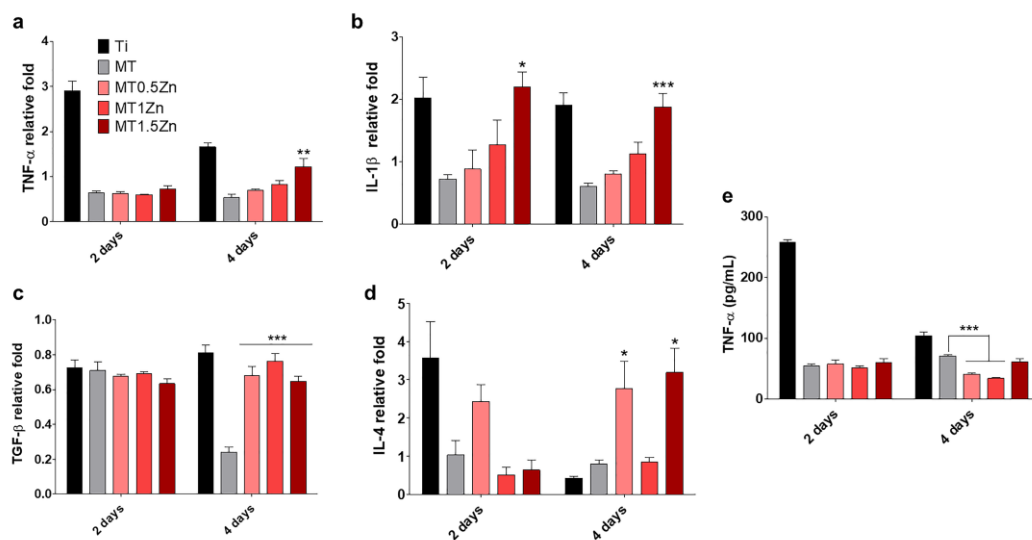


308
 309 **Fig. 6.** Gene expression of (a) ALP, (b) TGFβ, (c) iNOS, (d) RUNX2, (e) RANKL, and (f)
 310 RANK in MC3T3-E1 cells at 7 and 14 days of assay. Results are shown as mean ± SE. The
 311 asterisks ($p \leq 0.05$ (*), $p \leq 0.01$ (**), and $p \leq 0.001$ (***)) indicate statistically significant IL
 312 differences between the materials with Zn and the coating without Zn (MT). Data were
 313 normalized to blank wells (without any material) using the $2^{-\Delta\Delta C_t}$ method.

314 3.2.2. Inflammatory responses: effects on macrophages

315 Gene expression of RAW264.7 was examined to evaluate the effects of Zn-enriched sol-gel
 316 coatings on inflammatory-response markers (**Fig. 7**). After 2 days of incubation, there were no
 317 changes in pro- or anti-inflammatory marker levels with Zn-coatings, except in IL-1β, which
 318 presented a significant increase in MT1.5Zn (**Fig. 7b**). After 4 days, there was a significant
 319 increase in TNF-α and IL-1β gene expression on MT1.5Zn (**Fig. 7a and b**). An increase in the

320 expression of TGF β was seen on all the tested materials (**Fig. 7c**), while IL-4 showed an
 321 increase in MT0.5Zn and MT1.5Zn. The production of TNF- α by RAW264.7 cells was
 322 measured using ELISA (**Fig. 7e**). For the first two days, there were no differences between the
 323 materials. After 4 days, there was a significant decrease in TNF- α production on Zn-coatings
 324 (MT0.5Zn and MT1Zn) in comparison with the MT.



325
 326 **Fig. 7.** Gene expression of (a) TNF α , (b) IL-1 β , (c) TGF- β , and (d) IL-4, and (e) TNF- α cytokine
 327 liberation in RAW264.7 cells at 2 and 4 days of assay. Results are shown as mean \pm SE. The
 328 asterisks ($p \leq 0.05$ (*), $p \leq 0.01$ (**), and $p \leq 0.001$ (***)) indicate statistically significant
 329 differences between the materials with Zn and the coating without Zn (MT). Gene expression
 330 data were normalized to blank wells (without any material) using the $2^{-\Delta\Delta C_t}$ method.

331 3.2.3. Proteomic analysis

332 A total of 289 distinct proteins were identified in the elutions of the protein layers adsorbed
 333 onto the different materials. The comparative analysis using PEAKS detected 61 proteins
 334 differentially adsorbed onto the materials enriched with Zn (**Supplementary Table 1**).
 335 PANTHER and DAVID proteomic tools were employed to classify these proteins by their
 336 functions. The differentially adsorbed proteins and their functions associated with the
 337 regeneration process are listed in **Table 2**. Proteins associated with innate immunity and
 338 inflammation were detected in higher proportions on the surfaces with Zn. These were SAMP,
 339 CO4A, CO9, CXCL7, CO3, C1S, CO4B and immunoglobulins LAC3, IGJ, and IGKC, as well
 340 as FHR1, CLUS, IC1, and VTNC, which have regulatory/anti-inflammatory functions. A
 341 cluster of apolipoproteins, linked to lipid metabolism functions, also preferentially adsorbed
 342 onto Zn-containing coatings (APOF, APOL1, SAA4, APOC4, APOC3, APOC2, APOA2, and

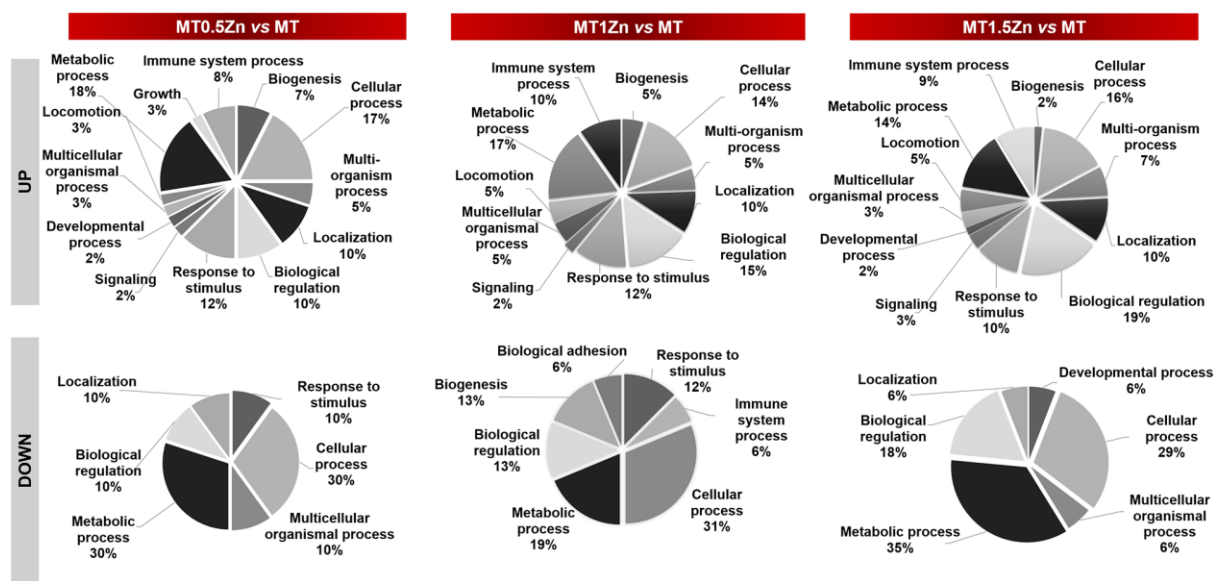
343 APOA1). HBB showed increased adsorption to MT0.5Zn and MT1Zn, while reduced amounts
 344 of HRG adhered to MT0.5Zn. These two proteins are associated with metal-binding and blood-
 345 clotting functions. Similarly, PLF4, PROC, and IPSP proteins, which showed increased affinity
 346 to the Zn-containing coatings, were linked to blood coagulation processes. VTNC was found
 347 more adsorbed to all the Zn-coatings than to the control surface. This glycoprotein is associated
 348 with regenerative functions, but also to blood clotting and the inhibition of immune response.
 349 In contrast, TITIN, a metal-binding protein with tissue regeneration functions, showed
 350 weakened adsorption onto MT0.5Zn. However, TITIN showed an augmented affinity to the
 351 coating doped with 1 % ZnCl₂. CERU and KAIN glycoproteins were most abundant on the
 352 coating with the highest amount of Zn. CERU is associated with metal-binding, while KAIN is
 353 a protease inhibitor. PRDX1, which has a peroxidase activity, showed a weakened affinity to
 354 the MT1Zn material, whereas CATB, associated with proteolysis, was less abundant on
 355 MT1.5Zn.

356 **Table 2.** Proteins with important functions in the bone tissue regeneration process differentially
 357 adsorbed onto the Zn-containing coatings. Proteins with $p \leq 0.05$ and a ratio higher than 1.3 in
 358 either direction (UP: increased and DOWN: reduced) were considered differentially adsorbed.

		MT0.5Zn vs MT	MT1Zn vs MT	MT1.5Zn vs MT
Immune responses	UP	FHR1, IGJ, SAMP, CO4A, CLUS, LAC3, C1S, IGKC	IGJ, SAMP, CO4A, CLUS, CO3, CO4B	FHR1, IGJ, SAMP, CO4A, CO9, CXCL7, CLUS, CO3, IC1
	DOWN	-	-	-
Apolipoproteins	UP	APOF, APOL1, SAA4, APOC4, APOC3, APOC2	APOF, APOL1, SAA4, APOA2, APOA1	APOF, APOL1, SAA4, APOC4, APOC2, APOA2
	DOWN	-	-	-
Blood coagulation	UP	HBB	PLF4, PROC, HBB	PLF4, IPSP
	DOWN	HRG	-	-
Osteogenesis	UP	VTNC	VTNC, TITIN	CERU, VTNC, KAIN
	DOWN	TITIN	PRDX1	CATB

359

360 The proteomic tool PANTHER was used to classify the differentially adsorbed proteins
 361 according to their participation in biological processes (**Fig. 8**). The proteins with increased
 362 adsorption to the Zn-containing coatings are associated with a wide range of different processes
 363 (such as biological regulation, response to a stimulus, developmental, locomotion, metabolic,
 364 cellular, multicellular, localization, biogenesis, signaling and immune system processes). In
 365 contrast, the proteins with reduced affinity to the Zn-coatings are mainly related to the response
 366 to stimulus, biological regulation, and metabolic, cellular and multicellular functions in
 367 biological processes. The biological adhesion and immune system functions were also
 368 associated with some of the proteins with reduced affinity to the MT1Zn material.



369
 370 **Fig. 8.** PANTHER functional classification of proteins differentially adsorbed onto the
 371 Zn-containing coatings in comparison with the control material MT. Proteins with $p \leq 0.05$ and
 372 a ratio higher than 1.3 in either direction (UP – increased and DOWN – reduced) were
 373 considered differentially adsorbed.

374 4. Discussion

375 The main aim of this study was to develop and characterize a new bioactive Zn-doped sol-gel
 376 coating for a Ti substrate. The effects of this element on protein adsorption and cellular
 377 responses in terms of osteogenesis and inflammation were evaluated. Zinc is an essential trace
 378 element with a stimulatory effect on bone growth and a pivotal role in bone maintenance. It has
 379 been described as the ‘calcium of the twenty-first century’ since Zn-containing biomaterials are
 380 showing great promise in applications for bone tissue regeneration [13].

381 The Zn-doped sol-gel coatings were obtained following the sol-gel route. The incorporation of
382 this compound did not affect the degree of crosslinking in the new sol-gel network or caused
383 significant differences in surface roughness of the new coatings. However, increasing the
384 amount of Zn in the sol-gel resulted in a significant reduction of the material hydrophilicity.
385 The material without Zn lost approximately 40 % of its mass after 63 days of incubation in
386 water. The incorporation of ZnCl₂ increased the hydrolytic degradation rate; the MT1.5Zn
387 composition lost around 50 % of its mass after the same period. A controlled Zn²⁺ release was
388 achieved as more Zn salt was incorporated into the network; the more Zn was liberated. The
389 release of this compound continued until the end of the essay (21 days), demonstrating
390 consistent long-term release properties. The quantified Zn²⁺ concentrations were less than 10
391 ppm in all the cases, not reaching the limit of cellular toxicity of 26.2 ppm defined by Brauer
392 *et al.* [31]. Moreover, *in vitro* results showed that these new Zn-containing coatings were not
393 cytotoxic to MC3T3-E1 cells.

394 The analysis of MC3T3-E1 osteogenic markers showed that RUNX2 expression, a member of
395 the runt domain family involved in bone development, was increased at 7 and 14 days.
396 Yamaguchi *et al.* [32] showed zinc sulphate upregulates the RUNX2 expression. This was
397 accompanied by the augmented ALP expression at 14 days in MT1.5Zn, whose activity is
398 activated by RUNX2 [33] and stimulated by Zn in MC3T3-E1 cells [6]. Additionally, TGF-β
399 gene expression was increased on MT0.5Zn and MT1.5Zn. This cytokine is critical in the
400 promotion of bone formation, as it plays roles in the recruitment of osteoblast, and enhancement
401 of osteoblast proliferation and differentiation [34], thus confirming the effects of these Zn-
402 doped coatings in the osteoblastic differentiation.

403 Inflammation is required to protect the host from tissue damage, which leads to the restoration
404 of homeostasis. The pro-inflammatory markers TNF-α and IL-1β [35] presented an increased
405 gene expression in MT1.5Zn after 4 days of culture, while, at the same time point, MT0.5Zn
406 and MT1Zn secreted significantly less TNF-α. Similarly, Giovanni *et al.* [36] developed zinc
407 oxide nanoparticles that lead to an increased fold change in TNF-α and IL-1β in a dose-response
408 manner. On the other hand, the overexpression of TGF-β and IL-4 [35], two anti-inflammatory
409 markers, in Zn-containing materials, confirming that the inflammatory responses might depend
410 on the used Zn concentration.

411 The phenomenon of protein adsorption onto a material can affect the initial biological healing
412 processes [37]. Therefore, studying how proteins are attached to a surface can help to predict a

413 biomaterial outcome. The nLC-MS/MS analysis identified significant changes in the patterns
414 of proteins adsorbed associated with increasing amounts of Zn incorporated onto the sol-gel
415 coating. Among the proteins found, a set belonging to a cluster related to the innate immune
416 system was identified, containing immunoglobulins and complement system proteins such as
417 C1S, CO3, CO4A, CO4B and CO9, which can activate the cascade of pro-inflammatory
418 response [20]. In general, these proteins tended to increase their attachment affinity to the
419 surfaces as more Zn was added to the sol-gel. However, a clear increase in the adsorption of
420 proteins associated with inhibitory/regulatory functions of complement cascade was also
421 observed. Proteins such as VTNC, IC1, FHR1, and CLUS, which showed augmented affinity
422 to Zn-enriched coatings, can control the complement system activation. They act as anti-
423 inflammatory factors [38]. The increased adsorption of this group of proteins is consistent with
424 the anti-inflammatory potential observed *in vitro*. Likewise, the increased attachment of
425 apolipoproteins onto the materials with Zn could affect the immune response regulation. This
426 protein family can prevent the initiation of innate immune response by inhibition of NF- κ B-
427 dependent gene expression [39].

428 Moreover, the VTNC can promote the macrophage polarization into the M2 pro-regenerative
429 phenotype [40]. This protein is associated with the coagulation system; it contributes to
430 thrombus formation and participates in vascular homeostasis and tissue regeneration [41].
431 VTNC is also involved in bone metabolism as it can promote the osteogenic differentiation of
432 mesenchymal stem cells [42]. It improves the bone healing capacity of Ti implants [43] and the
433 biomaterial vascularization process [44]. The rise in VTCN adsorption with increasing Zn
434 content in the coatings might be correlated with their increased osteogenic activity. Moreover,
435 TITIN, more abundant on the MT1Zn, has been associated with signaling in bone remodeling.
436 It has also been linked with an increase in cell proliferation of MG-63 osteoblasts via activation
437 of the Wnt/ β -catenin pathway [45]. Similarly, CXCL7, preferentially adsorbed onto MT1.5Zn,
438 can significantly stimulate the recruitment of human mesenchymal stem cells (MSC) *in vitro*
439 [46].

440 The studies of the role of Zn²⁺ in bone resorption have revealed that the osteoclasts are sensitive
441 to this ion; a significant decrease in bone resorption occurs at the concentration as low as 10⁻¹⁴
442 M [47]. Binding of RANKL to its receptor RANK activates NF- κ B, inducing osteoclast
443 differentiation. Zn²⁺ may reduce osteoclastogenesis via suppression of RANK expression
444 through prevention of oxidative stress species production [7]. In this study, no differences in
445 the expression RANKL were found. Similarly, Yusa et al. found that Zn did not affect RANKL

446 or OPG mRNA expression in zinc-modified titanium surfaces [33], which is consistent with
447 these results. However, RANK expression increased for MT1.5Zn; in parallel iNOS marker
448 resulted overexpressed for MT1Zn and MT1.5Zn. Thus, the effect of Zn-enriched materials on
449 osteoclastogenesis could depend on the added Zn concentration.

450 The proteomic results indicate that Zn could also affect the coagulation processes around the
451 implant materials. The proteins with pro-coagulant (VTNC, PLF4, IPSP, and HBB) and anti-
452 coagulant functions (PROC) showed increased adsorption to Zn-containing surfaces, in a Zn
453 dose-dependent manner. It is difficult to predict the real-life effect of these proteins on the
454 implant surface. Some studies have described a potential anticoagulation role of Zn-alloy
455 biomaterials [48,49]. However, it has also been reported that high concentrations of Zn²⁺ might
456 promote thrombosis [49].

457 Interestingly, CERU, an acute-phase protein with antioxidant properties, showed increased
458 adsorption to the surfaces with Zn (a 21-fold increase on the MT1.5Zn material in comparison
459 with the control surface). This protein is known as the main warehouse of plasma copper, but
460 it can also bind to Zn via its copper-binding sites [50]. Its augmented adsorption in MT1.5Zn
461 supports these findings. High levels of CERU in plasma have been associated with osteoporosis,
462 independently of other inflammatory parameters [51]. However, its role in this bone disease is
463 unknown. KAIN, which belongs to the serine proteinase inhibitor superfamily, was also
464 significantly more abundant on the MT1.5Zn surface. This protein exerts its anti-inflammatory
465 effect via the canonical Wnt pathway [52]. It can stimulate the M2 phenotype in cultured RAW
466 264.7 macrophages, causing overexpression of IL-10 [53]. However, KAIN plays a dual role
467 in angiogenesis. It inhibits the process by blocking VEGF-induced effects and TNF- α -induced
468 VEGF synthesis, but it can also stimulate neovascularization by increasing the levels of
469 endothelial nitric oxide synthase (eNOS) and VEGF [54].

470 The adsorption of the proteins CATB and PRDX1 was reduced on the MT1.5Zn and MT1Zn
471 surfaces (33-fold and 25-fold decrease), respectively. The peroxidase PRDX1 is associated with
472 various biological processes such as the detoxification of oxidants and cell apoptosis. Du *et al.*
473 have reported that the association between oestrogen and this protein might affect the osteoblast
474 cell responses to oxidative stress [55]. CATB is an enzyme involved in promoting chronic
475 inflammation, delaying tissue healing [56]. This protein is also responsible for NF-kB
476 activation via autophagy degradation of I κ B α in microglia/macrophages [57]. Moreover,
477 elevated levels of CATB are typically observed in many chronic inflammatory diseases,

478 including rheumatoid arthritis and periodontitis [58,59]. Thus, its diminished affinity to Zn-
479 containing biomaterials might have a positive effect on tissue regeneration.

480 **5. Conclusion**

481 New sol-gel materials doped with increasing amounts of Zn were applied as coatings onto Ti
482 discs, allowing the control of the release kinetics of this ion. The presence of Zn affected the *in*
483 *vitro* responses of osteoblasts and macrophages and protein adsorption onto the coated surfaces.
484 The levels of ALP, TGF- β , and RUNX2 gene expression in osteoblasts increased for the
485 materials with Zn, showing the osteogenic potential of these materials. The fold-changes in
486 TNF- α , IL-1 β , TGF- β and IL-4 show that the inflammatory responses these are dependent on
487 the amount of Zn is incorporated into the material. The nLC-MS/MS proteomic analysis
488 revealed that the addition of Zn significantly changed the attachment of proteins involved in
489 the immune, coagulation, and regenerative processes. Zinc sharply increased the adsorption of
490 proteins regulating the immune reaction, such as VTNC, IC1, FHR1, CLUS, and KAIN. In
491 contrast, it decreased the adsorption of CATB protein, which is associated with chronic
492 inflammation and delayed healing. Moreover, an increased proportion of proteins with
493 osteogenic function, such as VTNC, attached to the Zn-containing coatings. Thus, the
494 proteomic results were consistent with the biological responses observed *in vitro*. Our results
495 show the future possibility of clinical application of these new coatings to bioactivate Ti
496 prostheses.

497 **6. Acknowledgments**

498 This work was supported by MINECO [MAT2017-86043-R; RTC-2017-6147-1], Generalitat
499 Valenciana [GRISOLIAP/2018/091], Universitat Jaume I under [UJI-B2017-37,
500 Posdoc/2019/28], the University of the Basque Country under [GIU18/189] and Basque
501 Government under [PRE_2017_2_0044]. The authors would like to thank Raquel Oliver, Jose
502 Ortega and Iraide Escobés for their valuable technical assistance, and Antonio Coso (GMI-
503 Ilerimplant) for producing the titanium discs.

504

505 **7. References**

- 506 [1] B. Dalisson, J. Barralet, Bioinorganics and Wound Healing, Adv. Healthc. Mater.
507 1900764 (2019) 1–22. doi:10.1002/adhm.201900764.
- 508 [2] B. Pemmer, A. Roschger, A. Wastl, J.G. Hofstaetter, P. Wobrauschek, R. Simon, H.W.
509 Thaler, P. Roschger, K. Klaushofer, C. Strel, Spatial distribution of the trace elements
510 zinc, strontium and lead in human bone tissue, Bone. 57 (2013) 184–193.

- 511 doi:10.1016/j.bone.2013.07.038.
- 512 [3] T. Huang, G. Yan, M. Guan, Zinc homeostasis in bone: Zinc transporters and bone
513 diseases, *Int. J. Mol. Sci.* 21 (2020). doi:10.3390/ijms21041236.
- 514 [4] E. O'Neill, G. Awale, L. Daneshmandi, O. Umerah, K.W.H. Lo, The roles of ions on
515 bone regeneration, *Drug Discov. Today.* 23 (2018) 879–890.
516 doi:10.1016/j.drudis.2018.01.049.
- 517 [5] H. Yang, X. Qu, W. Lin, D. Chen, D. Zhu, K. Dai, Y. Zheng, Enhanced
518 Osseointegration of Zn-Mg Composites by Tuning the Release of Zn Ions with
519 Sacrificial Mg-Rich Anode Design, *ACS Biomater. Sci. Eng.* 5 (2019) 453–467.
520 doi:10.1021/acsbiomaterials.8b01137.
- 521 [6] H. Seo, Y. Cho, T. Kim, H. Shin, I. Kwun, Zinc may increase bone formation through
522 stimulating cell proliferation, alkaline phosphatase activity and collagen synthesis in
523 osteoblastic MC3T3-E1 cells, *Nutr. Res. Pract.* 4 (2010) 356–361.
524 doi:10.4162/nrp.2010.4.5.356.
- 525 [7] N. Amin, C.C.T. Clark, M. Taghizadeh, S. Djafarnejad, Zinc supplements and bone
526 health: The role of the RANKL-RANK axis as a therapeutic target, *J. Trace Elem.
527 Med. Biol.* 57 (2020) 126417. doi:10.1016/j.jtemb.2019.126417.
- 528 [8] A.S. Prasad, Discovery of Human Zinc Deficiency : Its Impact on, *Adv. Nutr.* 4
529 (2013) 176–190. doi:10.3945/an.112.003210.176.
- 530 [9] A.S. Prasad, Zinc is an antioxidant and anti-inflammatory agent : its role in human
531 health, *Front. Nutr.* 1 (2014) 1–10. doi:10.3389/fnut.2014.00014.
- 532 [10] A.S. Prasad, B. Bao, F.W. Beck, O. Kucuk, F.H. Sarkar, Antioxidant effect of zinc in
533 humans, *Free Radic. Biol. Med.* 37 (2004) 1182–1190.
534 doi:10.1016/j.freeradbiomed.2004.07.007.
- 535 [11] M. Jiménez, C. Abradelo, J. San Román, L. Rojo, Bibliographic review on the state of
536 the art of strontium and zinc based regenerative therapies. Recent developments and
537 clinical applications, *J. Mater. Chem. B.* 7 (2019) 1974–1985. doi:10.1039/c8tb02738b.
- 538 [12] R. Osorio, I. Cabello, M. Toledano, Bioactivity of zinc-doped dental adhesives, *J.
539 Dent.* 42 (2014) 403–412. doi:10.1016/j.jdent.2013.12.006.
- 540 [13] Y. Su, I. Cockerill, Y. Wang, Y.-X. Qin, L. Chang, Y. Zheng, D. Zhu, Zinc-Based
541 Biomaterials for Regeneration and Therapy, *Trends Biotechnol.* 37 (2019) 428–441.
542 doi:10.1016/J.TIBTECH.2018.10.009.
- 543 [14] A. Vishwakarma, N.S. Bhise, M.B. Evangelista, J. Rouwkema, M.R. Dokmeci, A.M.
544 Ghaemmaghami, N.E. Vrana, A. Khademhosseini, Engineering Immunomodulatory

- 545 Biomaterials To Tune the Inflammatory Response, *Trends Biotechnol.* 34 (2016) 470–
546 482. doi:10.1016/j.tibtech.2016.03.009.
- 547 [15] F. Romero-Gavilán, A.M. Sanchez-Pérez, N. Araújo-Gomes, M. Azkargorta, I. Iloro,
548 F. Elortza, M. Gurruchaga, I. Goñi, J. Suay, Proteomic analysis of silica hybrid sol-gel
549 coatings: a potential tool for predicting the biocompatibility of implants in vivo,
550 *Biofouling.* 33 (2017) 676–689. doi:10.1080/08927014.2017.1356289.
- 551 [16] J. Huang, Y. Yue, C. Zheng, Vroman effect of plasma protein adsorption to
552 biomaterials surfaces, *J. Biomed. Eng.* 16 (1999) 371–6.
- 553 [17] V. Nicolin, D. De Iaco, R. Valentini, Osteoimmunology represents a link between
554 skeletal and immune system, *Ital. J. Anat. Embryology.* 121 (2016) 37–42.
555 doi:10.13128/IJAE-18342.
- 556 [18] F. Romero Gavilán, N. Araújo-Gomes, A. Cerqueira, I. Garcia Arnáez, C. Martínez
557 Ramos, M. Azkargorta, I. Iloro, F. Elortza, M. Gurruchaga, J. Suay, I. Goñi, Proteomic
558 analysis of calcium-enriched sol-gel biomaterials, *JBIC J. Biol. Inorg. Chem.* 24 (2019)
559 563–574. doi:10.1007/s00775-019-01662-5.
- 560 [19] M.M. Markiewski, B. Nilsson, K.N. Ekdahl, T.E. Mollnes, J.D. Lambris, Complement
561 and coagulation : strangers or partners in crime ?, *Trends Immunol.* 28 (2007) 184–192.
562 doi:10.1016/j.it.2007.02.006.
- 563 [20] N. Araújo Gomes, F. Romero Gavilán, Y. Zhang, C. Martinez Ramos, F. Elortza, M.
564 Azkargorta, J.J. Martín de Llano, M. Gurruchaga, I. Goñi, J.J.J.P. Van Den Beucken, J.
565 Suay, Complement proteins regulating macrophage polarisation on biomaterials,
566 *Colloids Surfaces B Biointerfaces.* 181 (2019) 125–133.
567 doi:10.1016/j.colsurfb.2019.05.039.
- 568 [21] F. Romero-Gavilan, N. Araújo-Gomes, A.M. Sánchez-Pérez, I. García-Arnáez, F.
569 Elortza, M. Azkargorta, J.J.M. de Llano, C. Carda, M. Gurruchaga, J. Suay, I. Goñi,
570 Bioactive potential of silica coatings and its effect on the adhesion of proteins to
571 titanium implants, *Colloids Surfaces B Biointerfaces.* 162 (2017) 316–325.
572 doi:10.1016/j.colsurfb.2017.11.072.
- 573 [22] F. Romero-Gavilán, N.C. Gomes, J. Ródenas, A. Sánchez, F. , Mikel Azkargorta, Ibon
574 Iloro, I.G.A. Elortza, M. Gurruchaga, I. Goñi, and J. Suay, Proteome analysis of
575 human serum proteins adsorbed onto different titanium surfaces used in dental
576 implants, *Biofouling.* 33 (2017) 98–111. doi:10.1080/08927014.2016.1259414.
- 577 [23] M. Martinez-Ibañez, M.J. Juan-Diaz, I. Lara-Saez, A. Coso, J. Franco, M. Gurruchaga,
578 J. Suay Anton, I. Goñi, Biological characterization of a new silicon based coating

- 579 developed for dental implants, *J. Mater. Sci. Mater. Med.* 27 (2016).
580 doi:10.1007/s10856-016-5690-9.
- 581 [24] International Organization for Standardization, Biological evaluation of medical
582 devices - Part 5: Tests for in vitro cytotoxicity, 3 ED (2009) 42.
- 583 [25] International Organization for Standardization, Biological evaluation of medical
584 devices - Part 12: Sample preparation and reference materials, (2012).
- 585 [26] A. Cerqueira, F. Romero-Gavilán, N. Araújo-Gomes, I. García-Arnáez, C. Martínez-
586 Ramos, S. Ozturan, M. Azkargorta, F. Elortza, M. Gurruchaga, J. Suay, I. Goñi, A
587 possible use of melatonin in the dental field : Protein adsorption and in vitro cell
588 response on coated titanium, *Mater. Sci. Eng. C.* 116 (2020) 111262.
589 doi:10.1016/j.msec.2020.111262.
- 590 [27] H.N. Kim, S.K. Lee, Atomic structure and dehydration mechanism of amorphous
591 silica: Insights from ^{29}Si and ^1H solid-state MAS NMR study of SiO_2 nanoparticles,
592 *Geochim. Cosmochim. Acta.* 120 (2013) 39–64. doi:10.1016/j.gca.2013.05.047.
- 593 [28] M.J. Juan-Díaz, M. Martínez-Ibáñez, M. Hernández-Escolano, L. Cabedo, R.
594 Izquierdo, J. Suay, M. Gurruchaga, I. Goñi, Study of the degradation of hybrid sol–gel
595 coatings in aqueous medium, *Prog. Org. Coatings.* 77 (2014) 1799–1806.
596 doi:10.1016/j.porgcoat.2014.06.004.
- 597 [29] F. Romero-Gavilán, S. Barros-Silva, J. García-Cañadas, B. Palla, R. Izquierdo, M.
598 Gurruchaga, I. Goñi, J. Suay, Control of the degradation of silica sol-gel hybrid
599 coatings for metal implants prepared by the triple combination of alkoxysilanes, *J.*
600 *Non. Cryst. Solids.* 453 (2016) 66–73. doi:10.1016/j.jnoncrysol.2016.09.026.
- 601 [30] J.C. Almeida, A.G.B. Castro, J.J.H. Lancastre, I.M. Miranda Salvado, F.M.A. Margaça,
602 M.H.V. Fernandes, L.M. Ferreira, M.H. Casimiro, Structural characterization of
603 PDMS–TEOS–CaO–TiO₂ hybrid materials obtained by sol–gel, *Mater. Chem. Phys.*
604 143 (2014) 557–563. doi:10.1016/j.matchemphys.2013.09.032.
- 605 [31] D.S. Brauer, E. Gentleman, D.F. Farrar, M.M. Stevens, R.G. Hill, Benefits and
606 drawbacks of zinc in glass ionomer bone cements, *Biomed. Mater.* 6 (2011) 045007.
607 doi:10.1088/1748-6041/6/4/045007.
- 608 [32] M. Yamaguchi, M. Goto, S. Uchiyama, T. Nakagawa, Effect of zinc on gene
609 expression in osteoblastic MC3T3-E1 cells: Enhancement of Runx2, OPG, and
610 regucalcin mRNA expressions, *Mol. Cell. Biochem.* 312 (2008) 157–166.
611 doi:10.1007/s11010-008-9731-7.
- 612 [33] K. Yusa, O. Yamamoto, M. Iino, H. Takano, M. Fukuda, Z. Qiao, T. Sugiyama, Eluted

613 zinc ions stimulate osteoblast differentiation and mineralization in human dental pulp
614 stem cells for bone tissue engineering, *Arch. Oral Biol.* 71 (2016) 162–169.
615 doi:10.1016/j.archoralbio.2016.07.010.

616 [34] K. Janssens, P. Ten Dijke, S. Janssens, W. Van Hul, Transforming growth factor- β 1 to
617 the bone, *Endocr. Rev.* 26 (2005) 743–774. doi:10.1210/er.2004-0001.

618 [35] Q. Gu, H. Yang, Q. Shi, Macrophages and bone inflammation, *J. Orthop. Transl.* 10
619 (2017) 86–93. doi:10.1016/j.jot.2017.05.002.

620 [36] M. Giovanni, J. Yue, L. Zhang, J. Xie, C.N. Ong, D.T. Leong, Pro-inflammatory
621 responses of RAW264.7 macrophages when treated with ultralow concentrations of
622 silver, titanium dioxide, and zinc oxide nanoparticles, *J. Hazard. Mater.* 297 (2015)
623 146–152. doi:10.1016/j.jhazmat.2015.04.081.

624 [37] F. Romero-Gavilán, N. Araújo-Gomes, I. García-Arnáez, C. Martínez-Ramos, F.
625 Elortza, M. Azkargorta, I. Iloro, M. Gurruchaga, J. Suay, I. Goñi, The effect of
626 strontium incorporation into sol-gel biomaterials on their protein adsorption and cell
627 interactions, *Colloids Surfaces B Biointerfaces.* 174 (2019) 9–16.
628 doi:10.1016/J.COLSURFB.2018.10.075.

629 [38] T.E. Mollnes, M. Kirschfink, Strategies of therapeutic complement inhibition, *Mol.*
630 *Immunol.* 43 (2006) 107–121. doi:10.1016/j.molimm.2005.06.014.

631 [39] N.H. Cho, S.Y. Seong, Apolipoproteins inhibit the innate immunity activated by
632 necrotic cells or bacterial endotoxin, *Immunology.* 128 (2009) 479–486.
633 doi:10.1111/j.1365-2567.2008.03002.x.

634 [40] Z. Chen, T. Klein, R.Z. Murray, R. Crawford, J. Chang, C. Wu, Y. Xiao,
635 Osteoimmunomodulation for the development of advanced bone biomaterials, *Mater.*
636 *Today.* 19 (2016) 304–321. doi:10.1016/j.mattod.2015.11.004.

637 [41] D.I. Leavesley, A.S. Kashyap, T. Croll, M. Sivaramakrishnan, A. Shokoohmand, B.G.
638 Hollier, Z. Upton, Vitronectin - Master controller or micromanager?, *IUBMB Life.* 65
639 (2013). doi:10.1002/iub.1203.

640 [42] R.M. Salaszyk, W.A. Williams, A. Boskey, A. Batorsky, G.E. Plopper, Adhesion to
641 Vitronectin and Collagen I Promotes Osteogenic Differentiation of Human
642 Mesenchymal Stem Cells., *J. Biomed. Biotechnol.* 2004 (2004) 24–34.
643 doi:10.1155/S1110724304306017.

644 [43] C. Cho, S.Y. Jung, C.Y. Park, H.K. Kang, I.L. Yeo, B. Min, A Vitronectin-Derived
645 Bioactive Peptide Improves Bone Healing Capacity of SLA Titanium Surfaces,
646 *Materials (Basel).* 12 (2019) 1–11.

- 647 [44] M.E.T. Hessenauer, K. Lauber, G. Zuchriegel, B. Uhl, T. Hussain, M. Canis, S.
648 Strieth, A. Berghaus, C.A. Reichel, Acta Biomaterialia Vitronectin promotes the
649 vascularization of porous polyethylene biomaterials, Acta Biomater. 82 (2018) 24–33.
650 doi:10.1016/j.actbio.2018.10.004.
- 651 [45] J. Qi, L. Chi, S. Labeit, A.J. Banes, Nuclear localization of the titin Z1Z2Zr domain
652 and role in regulating cell proliferation, Am. J. Physiol. - Cell Physiol. 295 (2008) 975–
653 985. doi:10.1152/ajpcell.90619.2007.
- 654 [46] G. Kalwitz, M. Endres, K. Neumann, K. Skriner, J. Ringe, O. Sezer, M. Sittinger, T.
655 Häupl, C. Kaps, Gene expression profile of adult human bone marrow-derived
656 mesenchymal stem cells stimulated by the chemokine CXCL7, Int. J. Biochem. Cell
657 Biol. 41 (2009) 649–658. doi:10.1016/j.biocel.2008.07.011.
- 658 [47] B.S. Moonga, D.W. Dempster, Zinc is a potent inhibitor of osteoclastic bone resorption
659 in vitro, J Bone Min. Res. 10 (1995) 453–457.
- 660 [48] Y.X. Yin, C. Zhou, Y.P. Shi, Z.Z. Shi, T.H. Lu, Y. Hao, C.H. Liu, X. Wang, H.J.
661 Zhang, L.N. Wang, Hemocompatibility of biodegradable Zn-0.8 wt% (Cu, Mn, Li)
662 alloys, Mater. Sci. Eng. C. 104 (2019) 109896. doi:10.1016/j.msec.2019.109896.
- 663 [49] J. Ma, N. Zhao, D. Zhu, Endothelial Cellular Responses to Biodegradable Metal Zinc,
664 ACS Biomater. Sci. Eng. 1 (2015) 1174–1182. doi:10.1021/acsbiomaterials.5b00319.
- 665 [50] V.R. Samygina, A. V. Sokolov, G. Bourenkov, T.R. Schneider, V.A. Anashkin, S.O.
666 Kozlov, N.N. Kolmakov, V.B. Vasilyev, Rat ceruloplasmin: A new labile copper
667 binding site and zinc/copper mosaic, Metallomics. 9 (2017) 1828–1838.
668 doi:10.1039/c7mt00157f.
- 669 [51] E.Y. Karakas, A. Yetisgin, D. Cadirci, H. Sezen, R. Altunbas, F. Kas, M. Demir, T.
670 Ulas, Usefulness of ceruloplasmin testing as a screening methodology for geriatric
671 patients with osteoporosis, J. Phys. Ther. Sci. 28 (2016) 235–239.
672 doi:10.1589/jpts.28.235.
- 673 [52] X. Liu, B. Zhang, J.D. McBride, K. Zhou, K. Lee, Y. Zhou, Z. Liu, J.X. Ma,
674 Antiangiogenic and antineuroinflammatory effects of kallistatin through interactions
675 with the canonical wnt pathway, Diabetes. 62 (2013) 4228–4238. doi:10.2337/db12-
676 1710.
- 677 [53] L. Bing, Z. Sheng, C. Liu, L. Qian, Y. Wu, Y. Wu, G. Ma, Y. Yuyu, Kallistatin Inhibits
678 Atherosclerotic Inflammation by Regulating Macrophage Polarization, Hum. Gene
679 Ther. 30 (2019) 339–351.
- 680 [54] J. Chao, P. Li, L. Chao, Kallistatin: Double-edged role in angiogenesis, apoptosis and

- 681 oxidative stress, *Biol. Chem.* 398 (2017) 1309–1317. doi:10.1515/hsz-2017-0180.
- 682 [55] J. Du, W. Feng, J. Sun, C. Kang, N. Amizuka, M. Li, Ovariectomy upregulated the
683 expression of Peroxiredoxin 1 & 5 in osteoblasts of mice, *Sci. Rep.* 6 (2016) 1–11.
684 doi:10.1038/srep35995.
- 685 [56] X. Li, Z. Wu, J. Ni, Y. Liu, J. Meng, W. Yu, H. Nakanishi, Y. Zhou, Cathepsin B
686 Regulates Collagen Expression by Fibroblasts via Prolonging TLR2/NF- κ B Activation,
687 *Oxid. Med. Cell. Longev.* 2016 (2016). doi:10.1155/2016/7894247.
- 688 [57] J. Ni, Z. Wu, C. Peterts, K. Yamamoto, H. Qing, H. Nakanishi, The critical role of
689 proteolytic relay through cathepsins B and E in the phenotypic change of
690 microglia/macrophage, *J. Neurosci.* 35 (2015) 12488–12501.
691 doi:10.1523/JNEUROSCI.1599-15.2015.
- 692 [58] B. Tong, B. Wan, Z. Wei, T. Wang, P. Zhao, Y. Dou, Z. Lv, Y. Xia, Y. Dai, Role of
693 cathepsin B in regulating migration and invasion of fibroblast-like synoviocytes into
694 inflamed tissue from patients with rheumatoid arthritis, *Clin. Exp. Immunol.* 177
695 (2014) 586–597. doi:10.1111/cei.12357.
- 696 [59] S.W. Cox, B.M. Eley, M. Kiili, A. Asikainen, T. Tervahartiala, T. Sorsa, Collagen
697 degradation by interleukin-1 β -stimulated gingival fibroblasts is accompanied by
698 release and activation of multiple matrix metalloproteinases and cysteine proteinases,
699 *Oral Dis.* 12 (2006) 34–40. doi:10.1111/j.1601-0825.2005.01153.x.
- 700